

## Evidence for a local lattice distortion in Ca-doped $\text{LaMnO}_3$

T. A. Tyson

*Los Alamos National Laboratory, Los Alamos, New Mexico 87545*

J. Mustre de Leon

*Centro de Investigacion y de Estudios Avanzados del Instituto Politecnico Nacional—Merida, Merida, Yuc, 97310, Mexico*

S. D. Conradson, A. R. Bishop, J. J. Neumeier, H. Röder, and Jun Zang

*Los Alamos National Laboratory, Los Alamos, New Mexico 87545*

(Received 5 February 1996)

We have found that a significant change in the local structure of  $\text{La}_{2/3}\text{Ca}_{1/3}\text{MnO}_3$  occurs between 80 K and temperatures above the Curie temperature,  $T_c=270$  K. Near-edge x-ray-absorption spectra exhibits changes between 80 K and above  $T_c$ . X-ray-absorption fine structure reveals differences between the nearest-neighbor Mn-O bond distributions at 80 K and above  $T_c$ . The single-site distribution at low temperature becomes a complex, multi-site distribution above  $T_c$ . The observed change is consistent with proposed small polaron related local Jahn-Teller distortions for  $T>T_c$ . [S0163-1829(96)02721-X]

The manganese-based perovskites,  $\text{La}_{1-x}\text{A}_x\text{MnO}_3$  ( $\text{A}=\text{Ca}, \text{Sn}, \text{Ba}, \text{etc.}$ ), form a  $\text{Mn}^{3+}/\text{Mn}^{4+}$  mixed-valence system for  $x>0$ , which exhibit interesting and coupled magnetic and transport properties.<sup>1</sup> These materials are antiferromagnetic insulators for  $x$  less than  $\sim 0.2$ , ferromagnetic metals in the range  $x$  greater than  $\sim 0.2$  to  $x$  less than  $\sim 0.5$ , and revert to being ferromagnetic insulators for  $x$  greater than  $\sim 0.5$ . For  $x\approx 1/3$  these materials attain their highest Curie temperatures:  $T_c(33\% \text{ Ca})\approx 270$  K,  $T_c(33\% \text{ Ba})\approx 420$  K, and  $T_c(33\% \text{ Sr})\approx 440$  K, and largest magnetoresistance effect with values as large as 90% at 50 kOe.<sup>1-3</sup> The resistivity peaks near  $T_c$  and shows activated hopping (insulating behavior) above  $T_c$  while behaving as in dirty metals below  $T_c$ . Experimentally, it has been found that a direct relation exists between the resistivity and the bulk magnetization.<sup>4</sup>

The unusual magnetotransport properties sparked a long development of microscopic theoretical models of these transition-metal perovskites. The first model for the onset of ferromagnetism was proposed by Zener,<sup>5(a)</sup> and generalized by Anderson and Hasegawa,<sup>5(b)</sup> and de Gennes.<sup>5(c)</sup> This “double-exchange” (DE) model involved spin coupling between  $\text{Mn}^{3+}$  and  $\text{Mn}^{4+}$  next-nearest-neighbor ions with the conduction electrons mediating the interaction. Recently, it has been shown that the standard DE model yields an estimate of  $T_c$  too high by an order of magnitude, and is incompatible with resistivity data.<sup>6</sup> A strong electron-phonon interaction was proposed to play a central role in the understanding of these materials.<sup>6</sup> A model which explicitly includes electron-lattice interactions, via a Jahn-Teller (JT) lattice coupling to holes, has shown that lattice effects indeed decrease  $T_c$ , and also drive strong “small polaron” distortions for  $T>T_c$ .<sup>6,7</sup>

Very recent experiments support the view that the lattice plays an important role in these materials. It was found that Ca-doped materials exhibit a strong coupling between external pressure and resistivity.<sup>8</sup> In addition, it has been observed that a strong magnetic field produces an orthorhombic to rhombohedral structural transition in  $\text{La}_{0.83}\text{Sr}_{0.17}\text{MnO}_3$ .<sup>9</sup>

Moreover, changes in  $T_c$  and the magnetoresistance as  $\text{A}$  changes in size have been reported.<sup>10</sup> A detailed picture of the average crystalline structure and the local atomic structure is thus important for an understanding of these materials. In particular, it is essential to determine the details of the oxygen distribution and whether the observed magnetic phase transitions and change in resistivity are associated with global or local structural changes.

As a probe of local structure in these systems, we have measured the Mn  $K$ -edge x-ray-absorption fine structure (XAFS) of  $\text{La}_{2/3}\text{Ca}_{1/3}\text{MnO}_3$  and have obtained the near-neighbor Mn-O bond distribution at 80 K and at two temperatures [273 K and room temperature ( $\sim 293$  K)] above  $T_c=270$  K. We have observed a significant difference between the nearest-neighbor Mn-O distribution above and below  $T_c$ .

Samples of  $\text{La}_{2/3}\text{Ca}_{1/3}\text{MnO}_3$  were synthesized by reacting  $\text{La}_2\text{O}_3$ ,  $\text{MnO}_2$ , and  $\text{CaCO}_3$  at 1273 K for 20 h in an  $\text{Al}_2\text{O}_3$  crucible in air. The powders were reground and further reacted at 1523 K for 20 h three times, then fired a last time at 1573 K and cooled in air over 20 h. The samples were found to have a 65% theoretical density (ratio of measured density to that computed for this material based on its unit cell volume and formula weight). X-ray-diffraction analysis showed single-phase material. The resistivity exhibits a maximum at 270 K which tracks the onset of ferromagnetism in the susceptibility curve as shown in Fig. 1. XAFS samples were prepared by grinding the sample with sucrose and pressing the powder into an aluminum sample holder, which was attached to a cold finger of a cryostat. The cryostat was cooled with liquid nitrogen for measurements at  $T\approx 80$  K, with ice/water at  $T=273$  K, and finally set at ambient temperature ( $T\approx 20^\circ\text{C}$ ).

Spectra were measured at the Stanford Synchrotron Radiation Laboratory (SSRL) beam line 4-1, under dedicated synchrotron radiation production conditions. Si(220) crystals were used to monochromatize the x-ray beam. Harmonic rejection was accomplished by changing the relative alignment

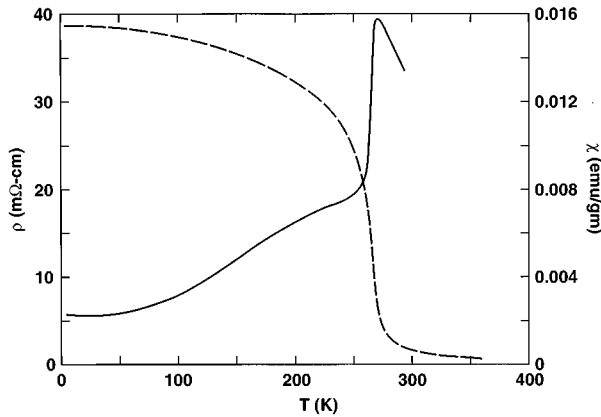


FIG. 1. Measured susceptibility  $\chi$  (dashed line) and resistivity  $\rho$  (solid line) as a function of temperature in  $\text{La}_{2/3}\text{Ca}_{1/3}\text{MnO}_3$ .

of the two crystals to reduce the flux to 50–60 % of its maximum level. Spectra were taken in fluorescence mode using an Ar-filled ion chamber. The reduction of the XAFS data was performed using standard procedures.<sup>11</sup> Calibration was accomplished by defining the first inflection point in the spectrum of Mn metal as 6538.3 eV, the ionization threshold,  $E_0$ , was set at 6560 eV, the photoelectron momentum is  $k = \sqrt{(2m/\hbar^2)(E - E_0)}$ . The data were normalized by setting the value of a second order polynomial fit over the preedge region to zero and the value of a third-order polynomial fit over the region above the edge to unity at  $E_0$ . After comparison, three individual scans were averaged for  $T=80$  and 273 K and five for room temperature (cf. inset, Fig. 2). The XAFS were extracted from the spectra as the difference between the normalized spectra and an adjustable spline function fit through the postedge region, the parameters of which were adjusted to minimize low frequency residuals in the Fourier transform.

Information about the Mn-O bond distribution was obtained by first fitting the  $k^3$  weighted raw data over the range  $3.7 < k < 11.0 \text{ \AA}^{-1}$ , including all shells through the Mn,<sup>12</sup> and subsequently subtracting the contributions for the higher

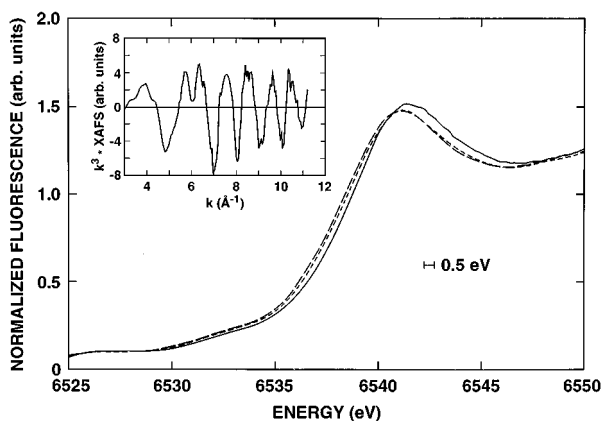


FIG. 2. X-ray-absorption near-edge structure of the Mn  $K$  edge at 80 K (solid line), 273 K (dotted line), and room temperature  $\sim 293$  K (dashed line). Inset shows typical raw x-ray-absorption fine-structure spectra at 273 K.

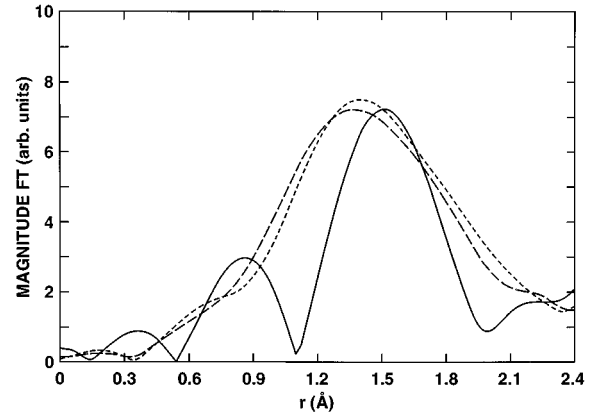


FIG. 3. (a) Magnitude of the Fourier transform of  $k^3 \cdot \text{XAFS}$  for  $k=3.7\text{--}10.8 \text{ \AA}^{-1}$  in the region of the oxygen near neighbors to Mn atoms at 80 K (solid line), 273 K (dotted line), and room temperature  $\sim 293$  K (dashed line). (b)  $k^3 \cdot \text{XAFS}$  spectra arising from Mn-O bonds at 80 K (solid line), 273 K (dotted line), and room temperature  $\sim 293$  K (dashed line).

shells from the raw XAFS and fitting just the residual Mn-O nearest-neighbor contribution. Potential problems with “leakage” were checked by iterating this procedure to produce consistent results.  $\Delta E_0$  was fixed at the value obtained from  $\text{MnO}_2$ . Photoelectron scattering factors utilized in these fits were obtained using the code FEFF6.<sup>13</sup> Radial distribution functions were obtained from the fits by summing individual Gaussian functions,  $g(r) = (N/\sqrt{2\pi}\sigma) e^{-(r-R)^2/2\sigma^2}$ , based on the average bond lengths,  $R$ , average coordination numbers,  $N$ , and Debye-Waller factors,  $\sigma$ , extracted from the fits.

As revealed in Fig. 2, the central position of the Mn  $K$ -edge x-ray-absorption near-edge structure (XANES) is  $\sim 0.5$  eV lower at temperatures above  $T_c$  than at 80 K. This observation is not typical temperature dependence but is indicative of changes in the local electronic and atomic structure between 80 K and the temperatures above  $T_c$ . The Fourier transform of the XAFS spectra over the region containing Mn nearest-neighbor oxygen atoms ( $R < 2.5 \text{ \AA}$ ) demonstrates that the distribution of oxygen nearest neighbors around the Mn ions at 80 K and at  $\sim 280$  K (above  $T_c$ ) is significantly different (see Fig. 3), in contrast to normal  $M$ -O bonds which have typical Debye frequencies of  $\sim 500$  K and exhibit minimal changes over this temperature range. All the other structural features in the transforms show only the expected decreases in amplitude resulting from increased fluctuation in bond lengths with increasing temperature.<sup>12</sup>

At 80 K, a single site with Gaussian distribution results in a good fit for the nearest-neighbor Mn-O contribution in the XAFS. In contrast, it is not possible to fit the spectra at  $\sim 280$  K using the single-site Gaussian disorder model. The precision to which the details of the Mn-O distribution could be determined was limited by the data range ( $k_{\text{max}} = 11.0 \text{ \AA}^{-1}$ ).

Consequently, rather than extract structural parameters based on an assumed but untestable Mn-O distribution, we obtained information about the general characteristics of the distribution. A large number of fits were performed, varying the number of shells and the parameters describing each shell. The results for the 273 and 293 K spectra are essentially identical. We found that the best fits, regardless of the

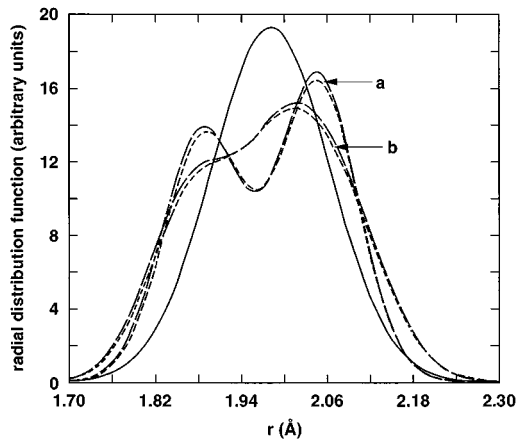


FIG. 4. Atomic Mn-O radial distributions functions at different temperatures. The solid line represents the single-shell bond distribution at 80 K while for curves (a) the long-dashed line is for a two-shell fit at 273 K and the short-dashed line is for a two-shell fit to the room-temperature data. For curves (b) the long-dashed lines are for a three-shell fit at 273 K and the short-dashed line is for a three-shell fit to the room-temperature data. The Debye-Waller factor of each shell was held fixed to reduce the number of parameters in the fits.

optimized fitting parameters, resulted in very similar radial distribution functions. The salient characteristics of the radial distributions at  $\sim 280$  K (Fig. 4) are (i) they are not the low-temperature structure modified by a wider Gaussian or asymmetric distribution, (ii) the extent (full width at half maximum) of the Mn-O bond distribution is 1.85–2.12 Å; (iii) the distribution is not just a two-site distribution (there is nonzero probability of finding Mn-O bonds at the minimum in the distribution), and (iv) there is an asymmetry between long and short bonds on the order of 1.3:1. This range of Mn-O distances is consistent with known Mn oxides.

This implication of the complex O distribution at  $\sim 280$  K and the change in this local structure at 80 K should have a significant effect on the magnetic and transport properties of these materials. At the higher temperature, which is above  $T_c$ , the charge carriers are apparently localized, inducing a local lattice (and spin) distortion (polaron) and leading to

hopping assisted conduction. At low temperatures the charge carriers are delocalized (dirty metal regime) resulting in a single type of O site. Although more measurements are required to ascertain whether this change in the structure is coincident with the metal-insulator transition, it is consistent with theoretical models predicting such a transformation in the nature of the carriers. Model calculations with plausible parameters for spring constants and electron-phonon coupling of a Jahn-Teller type yield the same order of magnitude as the distortion inferred from the XAFS data.<sup>7</sup> There is a strong coupling between spin, charge, and lattice degrees of freedom, and the small polaron formation is partly induced by the change of spin polarization around the charge carrier.<sup>7</sup> Theoretical studies also suggest that the JT distortion is homogeneous for  $T < T_c$  and inhomogeneous above  $T_c$  due to the formation of small polarons,<sup>6,7</sup> which at this doping ( $x = 1/3$ ) can form domains or superlattices. The observation of more than two Mn-O distances above  $T_c$  is inconsistent with a simple ordered arrangement of  $\text{Mn}^{3+}$  and  $\text{Mn}^{4+}$ . The possibility of polaron superlattice formation (commensurate or incommensurate) is currently under investigation, theoretically and experimentally.<sup>14</sup> This same issue is important in high-temperature superconducting cuprates which is another class of transition metal perovskites.<sup>15</sup> Experimentally, XAFS studies in the neighborhood of the Curie temperature will indicate whether abrupt changes in the structure track the loss of magnetic order. Additionally, the connection between magnetism and local structure could be probed by performing these measurements in the presence of a magnetic field. A systematic study of these temperature-dependent distortions for  $x$  values in the region  $x \sim 0.2$  and 0.5, and their correlation with optical, magnetic, and transport properties, will lead to a deeper understanding of the coupling between the magnetic, structural and charge degrees of freedom in these mixed-valence manganese based perovskites.

This work was performed under the auspices of the U.S. Department of Energy. Data acquisition was done at Stanford Synchrotron Radiation Laboratory, which is funded by the U.S. Department of Energy. J.M.L. acknowledges the support of Consejo Nacional de Ciencia y Tecnología Mexico, and the hospitality of Los Alamos National Laboratory.

<sup>1</sup>G. H. Jonker and J. H. van Santen, *Physica* **16**, 337 (1950); G. H. Jonker, *ibid.* **22**, 707 (1956); G. H. Jonker and J. H. van Santen, *ibid.* **16**, 49 (1954). See also Fig. 1 in H. L. Ju *et al.*, *Appl. Phys. Lett.* **65**, 2108 (1994).

<sup>2</sup>(a) S. Jin *et al.*, *Science* **264**, 413 (1994); (b) S. Jin, M. McCormack, T. H. Tiefel, and R. Ramesh, *J. Appl. Phys.* **76**, 6929 (1994).

<sup>3</sup>R. von Helmolt *et al.*, *Phys. Rev. Lett.* **71**, 2331 (1993); R. von Helmolt *et al.*, *J. Appl. Phys.* **76**, 6925 (1994).

<sup>4</sup>M. F. Hundley *et al.*, *Appl. Phys. Lett.* **67**, 860 (1995); R. Mahendiran *et al.*, *ibid.* **66**, 233 (1995).

<sup>5</sup>(a) C. Zener, *Phys. Rev.* **81**, 440 (1951); **82**, 403 (1951); (b) P. W. Anderson and H. Hasegawa, *ibid.* **100**, 675 (1955); (c) P.-G. de Gennes, *ibid.* **118**, 141 (1960).

<sup>6</sup>A. J. Millis, P. B. Littlewood, and B. I. Shraiman, *Phys. Rev. Lett.* **74**, 5144 (1995); A. J. Millis, B. I. Shraiman, and R. Mueller (unpublished).

<sup>7</sup>H. Roder, Jun Zang, and A. R. Bishop, *Phys. Rev. Lett.* **76**, 1356 (1996); J. Zang *et al.*, *Phys. Rev. B* **53**, R8840 (1996).

<sup>8</sup>(a) J. J. Neumeier *et al.* (unpublished); *Phys. Rev. B* **52**, R7006 (1995); *J. Magn. Magn. Mater.* **31-34**, 805 (1983); (b) Z. Arnold *et al.*, *Appl. Phys. Lett.* **67**, 2877 (1995); (c) Y. Morimoto, A. Asamitsu, and Y. Tokura, *Phys. Rev. B* **51**, 16 491 (1995); (d) S. Tamura, *J. Magn. Magn. Mater.* **31-34**, 675 (1982).

<sup>9</sup>A. Asamitsu *et al.*, *Nature* **373**, 407 (1995).

<sup>10</sup>H. Y. Hwang *et al.*, *Phys. Rev. Lett.* **75**, 914 (1995).

<sup>11</sup>P. A. Lee, P. H. Citrin, P. Eisenberger, and B. M. Kincaid, *Rev. Mod. Phys.* **53**, 679 (1981).

<sup>12</sup>T. A. Tyson *et al.* (unpublished). The Mn ( $R \sim 3.96 \text{ \AA}$ ) and La ( $R \sim 3.37 \text{ \AA}$ ) positions from the absorbing Mn ion are consistent with diffraction results in similar materials. We find that the Ca is displaced from the La site ( $R \sim 3.00 \text{ \AA}$ ). We also find two oxygen bonds at  $R \sim 2.50 \text{ \AA}$  and the four nearest-neighbor positions with  $R \sim 1.98 \text{ \AA}$  at 80 K and a more complex multishell distribution at temperatures above  $T_c$ . The observation of the longer of the Mn-O bonds implies a Mn-O-Mn angle significantly different from  $180^\circ$ , consistent with the results of Ref. 10. These longer oxygen bonds do not show significant changes with temperature. We also found these longer oxygen bonds in materials with different doping, or other cations, as well as the undoped parent material  $\text{LaMnO}_3$ . The local structural varia-

tions discussed in the text are with respect to this globally buckled structure. A statistical analysis of the differences in the amplitude envelopes of the low- and high-temperature data indicates a significance difference with a confidence level of 99%. Analysis of the Fourier-transformed data revealed that the spread in the individual scans is of the order of the difference between the 273 and 293 K data (Fig. 3 and Fig. 4)

<sup>13</sup>J. J. Rehr, S. I. Zabinsky, and R. C. Albers, *Phys. Rev. Lett.* **69**, 3397 (1992).

<sup>14</sup>A. P. Ramirez *et al.* (unpublished).

<sup>15</sup>A. Bianconi, *Solid State Commun.* **91**, 1 (1994); E. Pellegrini *et al.* (unpublished).